6. References

1. Fojo T, Grady C (2009) How much is life worth: cetuximab, non-small cell lung cancer, and the $440 billion question. J Natl Cancer Inst 101:1044-1048

2. Editorial (2008) Welcome clinical leadership at NICE. Lancet 372:601

3. Mayer RJ (2009) Targeted therapy for advanced colorectal cancer—more is not always better. N Engl J Med 360:623-625

4. Sinha G (2008) Expensive cancer drugs with modest benefit ignite debate over solutions. J Natl Cancer Inst 100:1347-1349

5. Tol J, Koopman M, Cats A et al (2009) Chemotherapy, bevacizumab, and cetuximab in metastatic colorectal cancer. N Engl J Med 360:563-572

6. From the Press Release material in Sankei Shinbun (2012) . March 3, New beptile therapy for pancreatic cancer

7. Oda T, Akaike T, Hamamoto T et al (1989) Oxygen radicals in influenza-induced pathogenesis and treatment with pyran polymer-conjugated SOD. Science 244:974-976

8. Akaike T, Ando M, Oda T et al (1990) Dependence on O_2^- generation by xanthine oxidase of pathogenesis of influenza virus infection in mice. J Clin Invest 85:739-745

9. Akaike T, Noguchi Y, Ijiri S, et al (1996) Pathogenesis of influenza virus-induced pneumonia: involvement of both nitric oxide and oxygen radicals. Proc Natl Acad Sci U S A 93:2448-2453

10. Akaike T, Okamoto S, Sawa T, et al (2003) 8-Nitroguanosine formation in viral pneumonia and its implication for pathogenesis. Proc Natl Acad Sci U S A 100:685-690

11. Yoshitake J, Akaike T, Akuta T, et al (2004) Nitric oxide as an endogenous mutagen for Sendai virus without antiviral activity. J Virol 78:8709-8719

12. Kuwahara H, Kariu T, Fang J, Maeda H (2009) Generation of drug-resistant mutants of *Helicobacter pylori* in the presence of peroxynitrite, a derivative of nitric oxide, at pathophysiological concentration. Microbiol Immunol 53:1-7

13. Sjöblom T, Jones S, Wood LD et al (2006) The consensus coding sequences of human breast and colorectal cancers. Science 314:268-274

14. Wood LD, Parsons W, Jones S et al (2007) The genomic landscapes of human breast and colorectal cancers. Science 318:1108-1113

15. Matsumura Y, Maeda H (1986) A new concept for macromolecular therapeutics in cancer chemotherapy: mechanism of tumoritropic accumulation of proteins and the antitumor agent smancs. Cancer Res 46:6387-6392

16. Noguchi Y, Wu J, Duncan R, et al (1998) Early phase tumor accumulation of macromolecules: a great difference in clearance rate between tumor and normal tissues. Jpn J Cancer Res 89:307-314

17. Seymour LW, Miyamoto Y, Maeda H, et al (1995) Influence of molecular weight on passive tumour accumulation of a soluble macromolecular drug carrier. Eur J Cancer 31A:766-770

18. Maeda H (2001) The enhanced permeability and retention (EPR) effect in tumor vasculature: the key role of tumor-selective macromolecular drug targeting. Adv Enzyme Regul 41:189-207

19. Fang J, Nakamura H, Maeda H (2011) The EPR effect: unique features of tumor blood vessels for drug delivery, factors involved, and limitations and augmentation of the effect. Adv Drug Deliv Rev 63:136-151

20. Maeda H, Fang J, Inutsuka T, Kitamoto Y (2003) Vascular permeability enhancement in solid tumor: various factors, mechanisms involved and its implications. Int Immunopharmacol 3:319-328

21. Wu J, Akaike T, Maeda H (1998) Modulation of enhanced vascular permeability in tumors by a bradykinin antagonist, a cyclooxygenase inhibitor, and a nitric oxide scavenger. Cancer Res 58:159-165

22. Maeda H, Bharate GY, Daruwalla J (2009) Polymeric drugs for efficient tumor-targeted drug delivery based on EPR-effect. Eur J Pharm Biopharm 71:409-419

23. Maeda H (2010) Tumor-selective delivery of macromolecular drugs via the EPR effect: background and future prospects. Bioconjug Chem 21:797-802

24. Maeda H (2012) Vascular permeability in cancer and infection as related to macromolecular drug delivery, with emphasis on the EPR effect for tumor-selective drug targeting. Proc Jpn Acad Ser B 88:53–71

25. Fang J, Qin H, Nakamura H, Tsukigawa K, Shin T, Maeda H (2012) Carbon monoxide, generated by heme oxygenase-1, mediates the enhanced permeability and retention effect in solid tumors. Cancer Sci 103:535-541

26. Konerding MA, Miodonski AJ, Lametschwandtner A (1995) Microvascular corrosion casting in the study of tumor vascularity: a review. Scanning Microsc 9:1233-1243; discussion 1243-1244

27. Hashizume H, Baluk P, Morikawa S, et al (2000) Openings between defective endothelial cells explain tumor vessel leakiness. Am J Pathol 156:1363-1380

28. Kimura NT, Taniguchi S, Aoki K, Baba T (1980) Selective localization and growth of *Bifidobacterium bifidum* in mouse tumors following intravenous administration. Cancer Res 40:2061-2068

29. Zhao M, Yang M, Li XM, et al (2005) Tumor-targeting bacterial therapy with amino acid auxotrophs of GFP-expressing *Salmonella typhimurium*. Proc Natl Acad Sci U S A 102:755-760

30. Hoffman RM (2009) Tumor-targeting amino acid auxotrophic *Salmonella typhimurium*. Amino Acids 37:509-521

31. Papillon J, Dargent M, Chassard JL (1963) [Ultra-fluid lipiodol lymphography in cancerology (apropos of 62 cases)]. J Radiol Electrol Med Nucl 44:397-406

32. Konno T, Maeda H, Iwai K, et al (1983) Effect of arterial administration of high-molecular-weight anticancer agent SMANCS with lipid lymphographic agent on hepatoma: a preliminary report. Eur J Cancer Clin Oncol 19:1053-1065

33. Konno T, Maeda H, Iwai K, et al (1984) Selective targeting of anti-cancer drug and simultaneous image enhancement in solid tumors by arterially administered lipid contrast medium. Cancer 54:2367-2374

34. Maki S, Konno T, Maeda H (1985) Image enhancement in computerized tomography for sensitive diagnosis of liver cancer and semiquantitation of tumor selective drug targeting with oily contrast medium. Cancer 56:751-757

35. Iwai K, Maeda H, Konno T (1984) Use of oily contrast medium for selective drug targeting to tumor: enhanced therapeutic effect and X-ray image. Cancer Res 44:2115-2121

36. Veronese FM, Pasut G (2005) PEGylation, successful approach to drug delivery. Drug Discov Today 10:1451-1458

37. Sahoo SK, Sawa T, Fang J, et al (2002) Pegylated zinc protoporphyrin: a water-soluble heme oxygenase inhibitor with tumor-targeting capacity. Bioconjug Chem 13:1031-1038

38. Ogino T, Inoue M, Ando Y, Awai M, Maeda H, Morino Y (1988) Chemical modification of superoxide dismutase. Extension of plasma half life of the enzyme through its reversible binding to the circulating albumin. Int J Pept Protein Res 32:153-159

39. Rutter DA, Wade HE (1971) The influence of the iso-electric point of L-asparaginase upon its persistence in the blood. Br J Exp Pathol 52:610-614

40. Kimura M, Matsumura Y, Konno T, Miyauchi Y, Maeda H (1990) Enzymatic removal of bilirubin toxicity by bilirubin oxidase in vitro and excretion of degradation products in vivo. Proc Soc Exp Biol Med 195:64-69

41. Fang J, Sawa T, Akaike T, Maeda H (2002) Tumor-targeted delivery of polyethylene glycol-conjugated D-amino acid oxidase for antitumor therapy via enzymatic generation of hydrogen peroxide. Cancer Res 62:3138-3143

42. Maeda H, Takeshita J, Kanamaru R (1979) A lipophilic derivative of neocarzinostatin. A polymer conjugation of an antitumor protein antibiotic. Int J Pept Protein Res 14:81-87

43. Kojima Y, Haruta A, Imai T, Otagiri M, Maeda H (1993) Conjugation of Cu,Zn-superoxide dismutase with succinylated gelatin: pharmacological activity and cell-lubricating function. Bioconjug Chem 4:490-498

44. Hirano T, Todoroki T, Kato S et al (1994) Synthesis of the conjugate of superoxide dismutase with the copolymer of divinylether and maleic anhydride retaining enzymatic activity. J Cont Release 28: 203-209

45. Maeda H (2001) SMANCS and polymer-conjugated macromolecular drugs: advantages in cancer chemotherapy. Adv Drug Deliv Rev 46:169-185

46. Maeda H, Matsumura Y (1989) Tumoritropic and lymphotropic principles of macromolecular drugs. Crit Rev Ther Drug Carrier Syst 6:193-210

47. Greish K, Fang J, Inutsuka T, Nagamitsu A, Maeda H (2003) Macromolecular therapeutics: advantages and prospects with special emphasis on solid tumour targeting. Clin Pharmacokinet 42:1089-1105

48. Zhang JS, Liu F, Huang L (2005) Implications of pharmacokinetic behavior of lipoplex for its inflammatory toxicity. Adv Drug Deliv Rev 57:689-698

49. Dash PR, Read ML, Barrett LB, Wolfert MA, Seymour LW (1999) Factors affecting blood clearance and in vivo distribution of polyelectrolyte complexes for gene delivery. Gene Ther 6:643-650

50. Kwoh DY, Coffin CC, Lollo CP, et al (1999) Stabilization of poly-L-lysine/DNA polyplexes for in vivo gene delivery to the liver. Biochim Biophys Acta 1444:171-190

51. He C, Hu Y, Yin L, Tang C Yin C (2010) Effects of particle size and surface charge on cellular uptake and biodistribution of polymeric nanoparticles. Biomaterials 31:3657-3666

52. Daruwalla J, Nikfarjam M, Greish K, et al (2010) In vitro and in vivo evaluation of tumor targeting styrene-maleic acid copolymer-pirarubicin micelles: survival improvement and inhibition of liver metastases. Cancer Sci 101:1866-1874

53. Li CJ, Miyamoto Y, Kojima Y, Maeda H (1993) Augmentation of tumour delivery of macromolecular drugs with reduced bone marrow delivery by elevating blood pressure. Br J Cancer 67:975-980

54. Nagamitsu A, Greish K, Maeda H (2009) Elevating blood pressure as a strategy to increase tumor-targeted delivery of macromolecular drug SMANCS: cases of advanced solid tumors. Jpn J Clin Oncol 39:756-766

55. Suzuki M, Hori K, Abe I, Saito S, Sato H (1981) A new approach to cancer chemotherapy: selective enhancement of tumor blood flow with angiotensin II. J Natl Cancer Inst 67:663-669

56. Suzuki M, Hori K, Abe I, et al (1984) Functional characterization of the microcirculation in tumors. Cancer Metastasis Rev 3: 115-126

57. Noguchi A, Takahashi T, Yamaguchi T, et al (1992) Enhanced tumor localization of monoclonal antibody by treatment with kininase II inhibitor and angiotensin II. Jpn J Cancer Res 83:240-243

58. Jain RK (1990) Physiological barriers to delivery of monoclonal antibodies and other macromolecules in tumors. Cancer Res 50:814s-819s

59. Hori K, Suzuki M, Tanda S (1991) Fluctuations in tumor blood flow under normotension and the effect of angiotensin II-induced hypertension. Cancer Sci 82:1309-1316

60. Matsumoto K, Yamamoto T, Kamata R, Maeda H (1984) Pathogenesis of serratial infection: activation of the Hageman factor-prekallikrein cascade by serratial protease. J Biochem 96:739-749

61. Kamata R, Yamamoto T, Matsumoto K, Maeda H (1985) A serratial protease causes vascular permeability reaction by activation of the Hageman factor-dependent pathway in guinea pigs. Infect Immun 48:747-753

62. Maeda H, Matsumura Y, Kato H (1988) Purification and identification of [hydroxyprolyl$_3$]bradykinin in ascitic fluid from a patient with gastric cancer. J Biol Chem 263:16051-16054

63. Matsumura Y, Maruo K, Kimura M, Yamamoto T, Konno T, Maeda H (1991) Kinin-generating cascade in advanced cancer patients and in vitro study. Jpn J Cancer Res 82:732-741

64. Matsumura Y, Kimura M, Yamamoto T, Maeda H (1988) Involvement of the kinin-generating cascade in enhanced vascular permeability in tumor tissue. Jpn J Cancer Res 79:1327-1334

65. Cohen RA, Adachi T (2006) Nitric-oxide-induced vasodilatation: regulation by physiologic S-glutathiolation and pathologic oxidation of the sarcoplasmic endoplasmic reticulum calcium ATPase. Trends Cardiovasc Med 16:109-114

66. Lincoln TM (1989) Cyclic GMP and mechanisms of vasodilation. Pharmacol Ther 41:479-502

67. Doi K, Akaike T, Horie H, et al (1996) Excessive production of nitric oxide in rat solid tumor and its implication in rapid tumor growth. Cancer 77:1598-1604

68. Maeda H (2010) Nitroglycerin enhances vascular blood flow and drug delivery in hypoxic tumor tissues: analogy between angina pectoris and solid tumors and enhancement of the EPR effect. J Control Release 142:296-298

69. Seki T, Fang J, Maeda H (2009) Enhanced delivery of macromolecular antitumor drugs to tumors by nitroglycerin application. Cancer Sci 100:2426-2430

70. Jordan BF, Misson P, Demeure R, Baudelet C, Beghein N, Gallez B (2000) Changes in tumor oxygenation/perfusion induced by the NO donor, isosorbide dinitrate, in comparison with carbogen: monitoring by EPR and MRI. Int J Radiat Oncol Biol Phys 48:565-570

71. Yasuda H, Nakayama K, Watanabe M, et al (2006) Nitroglycerin treatment may enhance chemosensitivity to docetaxel and carboplatin in patients with lung adenocarcinoma. Clin Cancer Res 12:6748-6757

72. Riganti C, Miraglia E, Viarisio D, et al (2005) Nitric oxide reverts the resistance to doxorubicin in human colon cancer cells by inhibiting the drug efflux. Cancer Res 65:516-525

73. Janssens MY, Van den Berge DL, Verovski VN et al (1998) Activation of inducible nitric oxide synthase results in nitric oxide-mediated radiosensitization of hypoxic EMT-6 tumor cells. Cancer Res 58: 5646-5648

74. Yasuda H, Yamaya M, Nakayama K, et al (2006) Randomized phase II trial comparing nitroglycerin plus vinorelbine and cisplatin with vinorelbine and cisplatin alone in previously untreated stage IIIB/IV non-small-cell lung cancer. J Clin Oncol 24:688-694

75. Hagen TL, Eggermont AM (2004) Tumor vascular therapy with TNF: critical review on animal models. Methods Mol Med 98:227-246

76. Blum MS, Toninelli E, Anderson JM, et al (1997) Cytoskeletal rearrangement mediates human microvascular endothelial tight junction modulation by cytokines. Am J Physiol 273:H286-294

77. Romer LH, McLean NV, Yan HC et al (1995) IFN-gamma and TNF-alpha induce redistribution of PECAM-1 (CD31) on human endothelial cells. J Immunol 154:6582-6592

78. Lampugnani MG, Resnati M, Raiteri M, et al (1992) A novel endothelial-specific membrane protein is a marker of cell-cell contacts. J Cell Biol 118:1511-1522

79. Folli S, Pelegrin A, Chalandon Y, et al (1993) Tumor-necrosis factor can enhance radio-antibody uptake in human colon carcinoma xenografts by increasing vascular permeability. Int J Cancer 53:829-836

80. Seki T, Carroll F, Illingworth S et al (2011) Tumour necrosis factor-alpha increases extravasation of virus particles into tumour tissue by activating the Rho A/Rho kinase pathway. J Control Release 156:381-389

81. van Nieuw Amerongen GP, Vermeer MA, Negre-Aminou P et al (2000) Simvastatin improves disturbed endothelial barrier function. Circulation 102:2803-2809

82. de Wilt JH, ten Hagen TL, de Boeck G et al (2000) Tumour necrosis factor alpha increases melphalan concentration in tumour tissue after isolated limb perfusion. Br J Cancer 82:1000-1003

83. van der Veen AH, de Wilt JH, Eggermont AM et al (2000) TNF- α augments intratumoural concentrations of doxorubicin in TNF- α -based isolated limb perfusion in rat sarcoma models and enhances anti-tumour effects. Br J Cancer 82:973-980

84. Roberts AB, Wakefield LM (2003) The two faces of transforming growth factor beta in carcinogenesis. Proc Natl Acad Sci U S A 100:8621-8623

85. Sofuni A, Iijima H, Moriyasu F, et al (2005) Differential diagnosis of pancreatic tumors using ultrasound contrast imaging. J Gastroenterol 40:518-525

86. Takahashi Y, Cleary KR, Mai M et al (1996) Significance of vessel count and vascular endothelial growth factor and its receptor (KDR) in intestinal-type gastric cancer. Clin Cancer Res 2:1679-1684

87. Kano MR, Bae Y, Iwata C et al (2007) Improvement of cancer-targeting therapy, using nanocarriers for intractable solid tumors by inhibition of TGF-beta signaling. Proc Natl Acad Sci U S A 104:3460-3465

88. Minowa T, Kawano K, Kuribayashi H et al (2009) Increase in tumour permeability following TGF- ・ type I receptor-inhibitor treatment observed by dynamic contrast-enhanced MRI. Br J Cancer 101:1884-1890

89. Kohmoto J, Nakao A, Kaizu T et al (2006) Low-dose carbon monoxide inhalation prevents ischemia/reperfusion injury of transplanted rat lung grafts. Surgery 140:179-185

90. Nakao A, Neto JS, Kanno S et al (2005) Protection against ischemia/reperfusion injury in cardiac and renal transplantation with carbon monoxide, biliverdin and both. Am J Transplant 5:282-291

91. Abraham NG, Kappas A. (2008) Pharmacological and clinical aspects of heme oxygenase. Pharmacol Rev 60:79-127

92. Doi K, Alaike T, Fujii S et al (1999) Induction of haem oxygenase-1 by nitric oxide and ischaemia in experimental solid tumours and implications for tumour growth. Br J Cancer 80:1945-1954

93. Maeda H (2012) Macromolecular therapeutics in cancer treatment: the EPR effect and beyond, J Control Release, in press

94. Maeda H, Matsumura Y, Oda T, Sasamoto K (1986) Cancer selective macromolecular therapeusis; tailoring of an antitumor protein drug. *In*: Feeney RE, Whitaker JR (eds): Protein tailoring for food and medical uses. Marcel Dekker, New York

95. Davis S, Abuchowski A, Park YK, Davis FF (1981) Alteration of the circulating life and antigenic properties of bovine adenosine deaminase in mice by attachment of polyethylene glycol. Clin Exp Immunol 46:649-652

96. Ensor CM, Holtsberg FW, Bomalaski JS, Clark MA (2002) Pegylated arginine deiminase (ADI-SS PEG20,000 mw) inhibits human melanomas and hepatocellular carcinomas in vitro and in vivo. Cancer Res 62:5443-5450

97. Zhao W, Zhuang S Qi XR (2011) Comparative study of the in vitro and in vivo characteristics of cationic and neutral liposomes. Int J Nanomed 6:3087-3098

98. Maeda H, Kimura I, Sasaki Y et al (1992) Toxicity of bilirubin and detoxification by PEG-bilirubin oxidase conjugate: A new tactic for treatment of jaundice. *In*: J. M. Harris (ed): Poly(Ethylene Glycol) Chemistry: Biotech Biomed Applications, Plenum Press, New York, p. 153-169

99. Kimura M, Matsumura Y, Miyauchi Y and Maeda H (1988) A new tactic for the treatment of jaundice: An injectable polymer-conjugated bilirubin oxidase. Proc Soc Exp Biol Med 188: 364-369

100. Li CY, Shan S, Huang Q etal (2000) Initial Stage of Tumor Cell-Induced Angiogenesis: Evaluation Via Skin Window Chambers in Rodent Models. J Natl Cancer Inst 92: 143-147

Figure 1

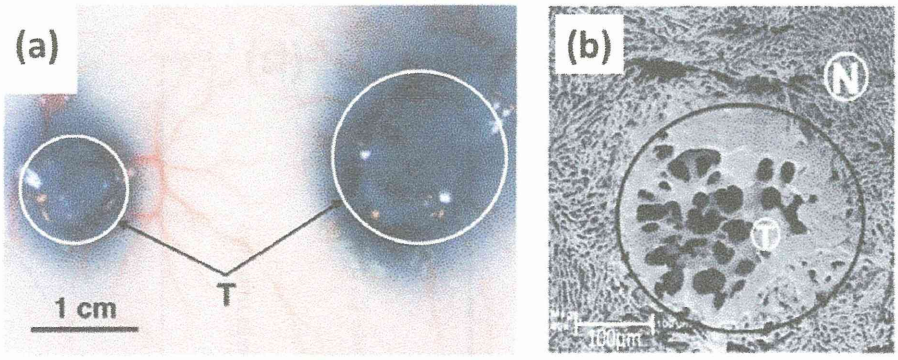

Fig. 1. Illustration of the EPR effect. (a) Tumor-selective accumulation of the putative macromolecular drug Evans blue-albumin complex (MW 67 kDa). The blue color in the macroscopic image indicates macromolecular drug delivery to S-180 tumor implanted in the skin of mice at 24 h after i.v. injection of Evans blue (10 mg/kg). The tumor sites (T, circles, and arrows) show progressive accumulation of Evans blue-albumin, in both small and large tumor. (b) Scanning electron microscopic image of metastatic liver cancer. The tumor (T, circle) is a micrometastatic tumor nodule; even this small nodule shows leakage of a polymer (polyarylate), which is not seen in the surrounding normal tissue (N, in the liver). (Adapted from refs [23]). Dewhirst et al showed that tumor angiogenesis becomes visible when 100-300 tumor cells present [100].

Figure 2.

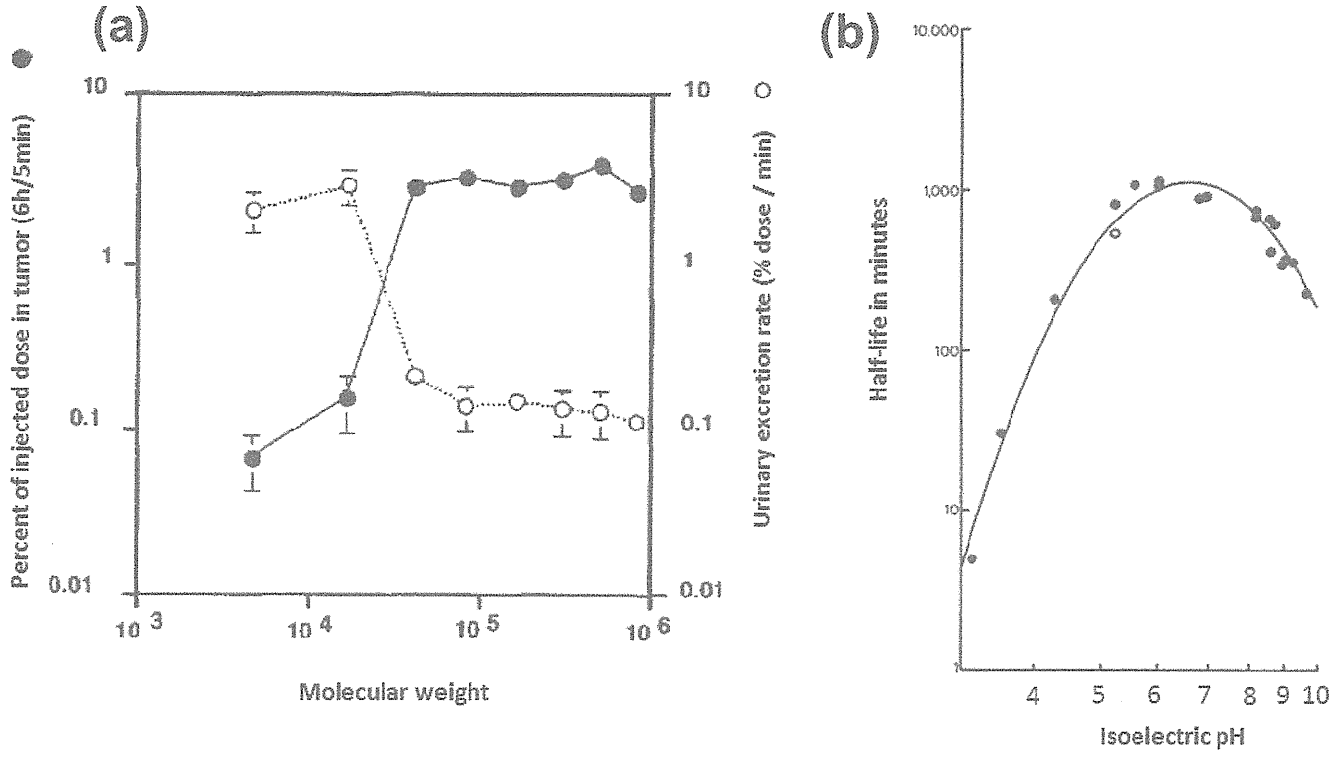

Fig. 2. Influence of the size and charge of macromolecules on their distribution in tumors and plasma concentration. (a) HPMA copolymers, labeled with ^{125}I and of different sizes, were injected i.v. into tumor-bearing mice. The percentage of the injected dose of HPMA in tumor and in urine was calculated. (Adapted from ref [16,23,24]). (b) L-Asparaginase derivatives (MW 120 kDa) with different isoelectric points (pI) after chemical modification were injected i.v. into rabbits (2500 IU/kg), after which the remaining activity of each L-asparaginase derivative was measured and their half-life values in systemic circulation were calculated. (Adapted from ref [39])

Figure 3

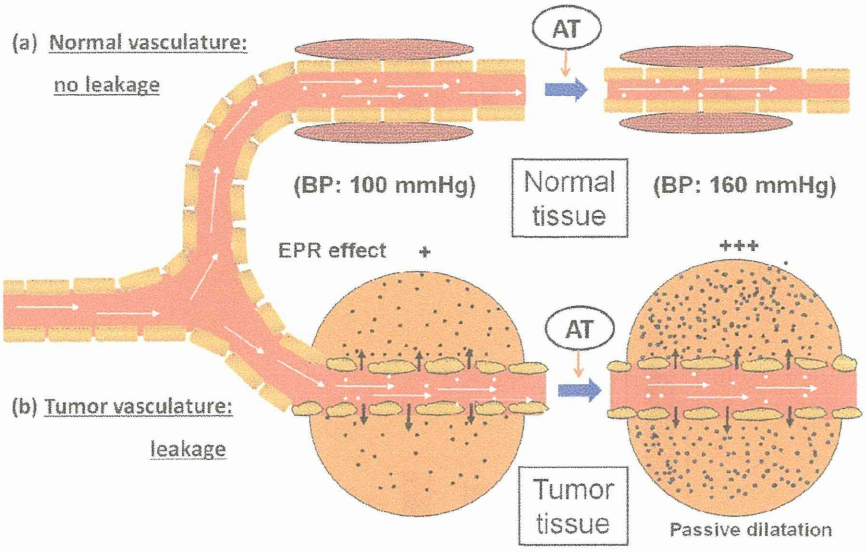

Fig. 3. Diagrammatic representation of the EPR effect and the effect of AT-II-induced enhancement of macromolecular drug delivery to normal and tumor tissue. In the lower part (tumor tissue), angiotensin II (AT-II) infusion induced high blood pressure (e.g., 100 mmHg → 160 mmHg), which caused endothelial cell-cell junctions in the tumor to open and blood flow to increase, with leakage of the macromolecular drug (dark dots). In contrast, normal blood vessels (upper part) constricts in response to AT-II, and tighten the endothelial cell-cell junctions that cause high blood pressure, with no leakage of the drug. AT-II-induced hypertension thus resulted in greater (2–3 fold) leakage of drug into the tumor without increased drug accumulation into normal tissue. (Adapted from ref [24])

Figure 4

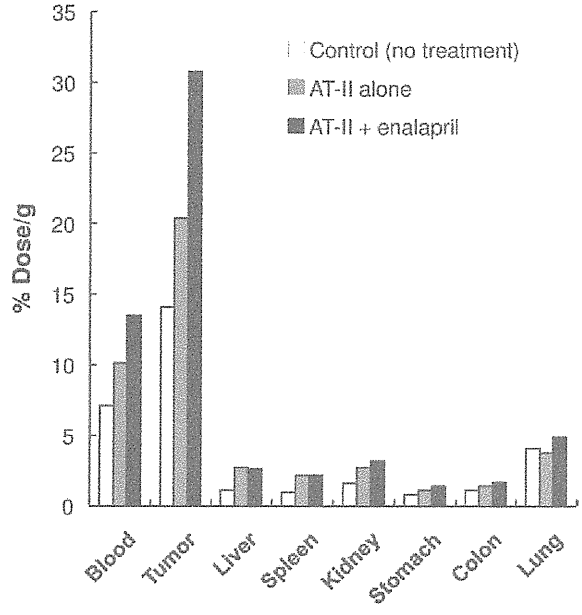

Fig. 4. Augmentation of the EPR effect and delivery of monoclonal antibody to the tumor by using AT-II and the ACE inhibitor enalapril. Human SW1116 colon cancer-bearing nude mice were injected i.v. with ^{125}I-labeled monoclonal antibody A7 with or without AT-II and enalapril. (Adapted from ref [57])

Figure 5

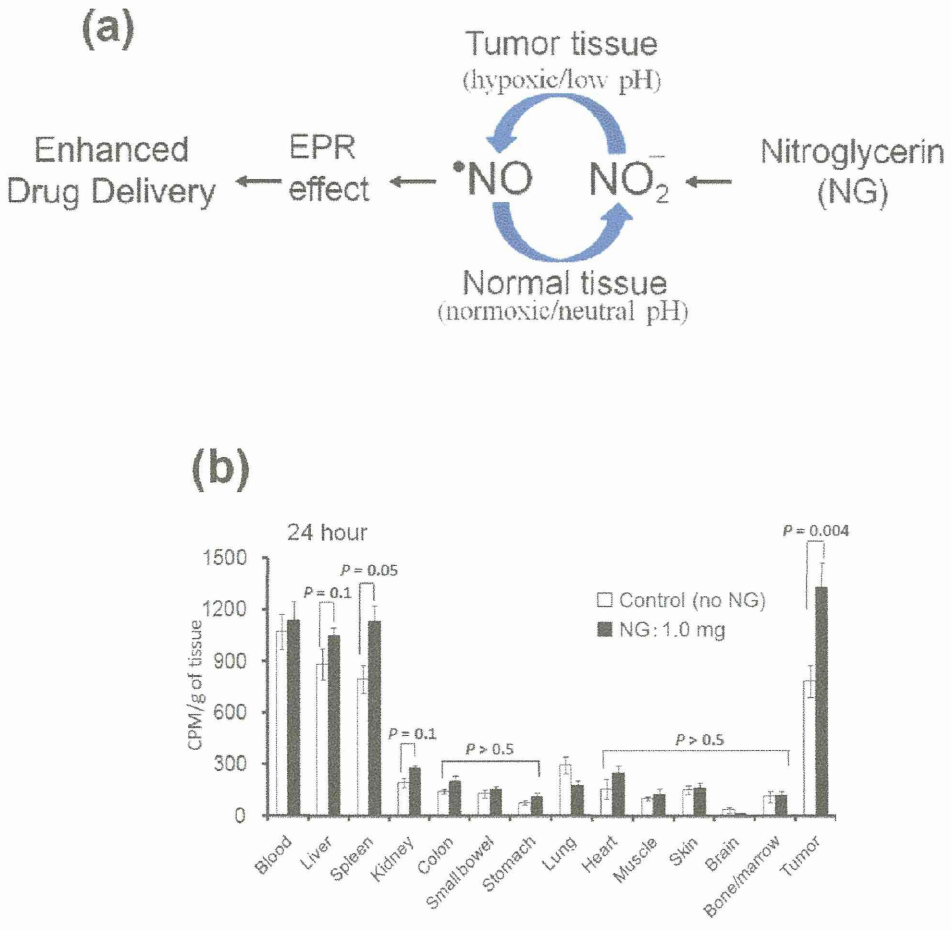

Fig. 5. Nitroglycerin (NG)-induced increase in accumulation of polymer-conjugated drug in tumors. (a) Mechanism of selective NO generation in tumor. NO was generated from nitrite, predominantly in hypoxic tumor tissue, not in normal tissue. (b) In vivo evaluation of the potentiation of drug delivery to tumor by nitroglycerin that was applied as an ointment to anywhere on the skin of S-180 tumor-bearing mice at a dose of 1.0 mg/mouse. Pegylated-^{65}Zn-labeled Zn-protoporphyrin was then injected i.v. into the tumor-bearing mice. After 24 h, anesthetized mice were dissected and radioactivity of each tissue was counted. (Adapted from refs [23,69])

Figure 6

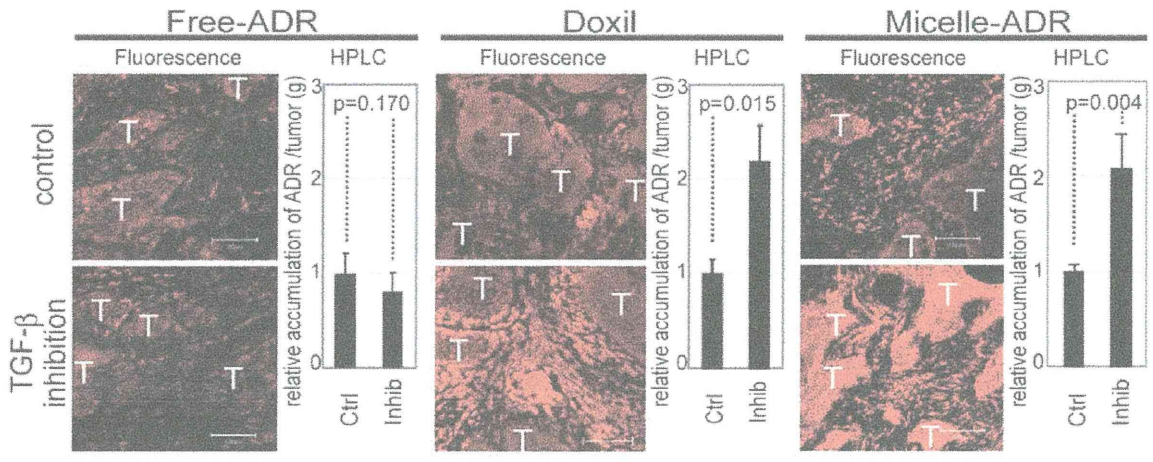

Fig. 6. Biodistribution of free ADR, Doxil, and ADR-micelles in the pancreatic cancer BxPC3 model in mice. Distributions of free ADR, Doxil, and ADR-micelles (each at 8 mg/kg) with or without TGF-β receptor inhibitor (LY364947) (1 mg/kg) were evaluated via fluorescent microscopy at 24 h after drug administration. Bar graphs at the right show relative quantitative results for the accumulation of drugs in tumors obtained by high-performance liquid chromatography (HPLC). Treatment with TGF-β receptor inhibitor resulted in about a two-fold enhancement of accumulation of Doxil and ADR micelles. Error bars in the graphs represent standard errors; *P* values were calculated by using Student's *t* test. T, nests of tumor cells in tumor tissues; Doxil, pegylated liposome; Ctrl, control without the inhibitor; Inhib, inhibitor. See text for detail. (Adapted from ref [87])

Figure 7

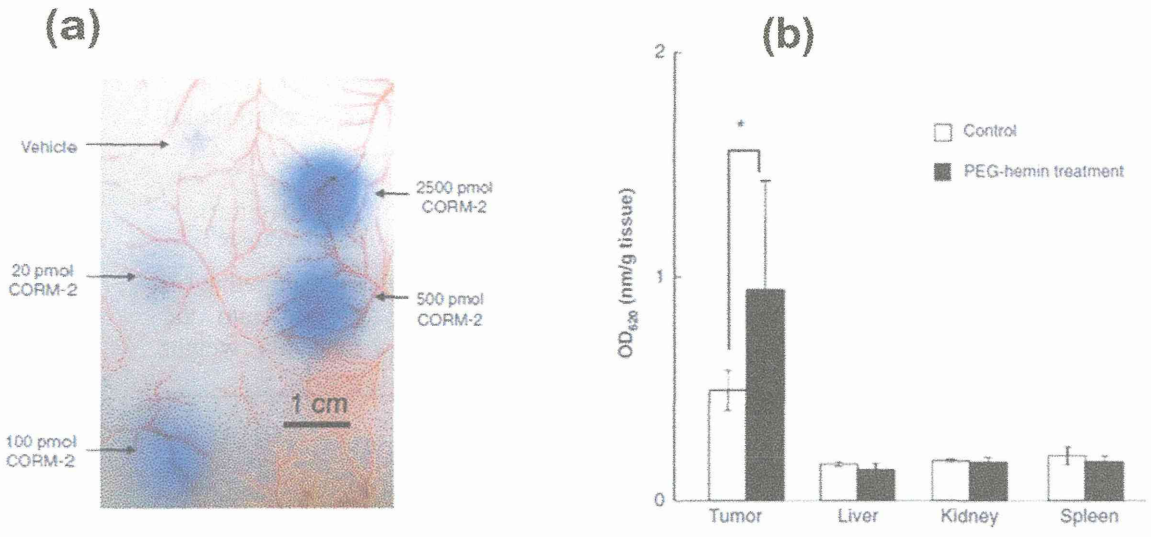

Fig. 7. CO-enhanced accumulation of Evans blue-albumin complex in tumors. (a) Different concentrations of the CO-releasing agent CORM-2 were administered subcutaneously, followed by i.v. injection of Evans blue (10 mg/kg). The dye-albumin complex was allowed to extravasate for 2 h. (b) At 24 h after the i.v. injection of an HO-1 inducer, pegylated hemin (10 mg/kg hemin equivalent), Evans blue was injected as in (a). After another 24 h, mice were killed and dissected to obtain the tissues. Control mice were not treated with pegylated hemin. The blue dye complexed with albumin in each tissue was extracted with formamide, and the degree of extravasation was quantified by means of absorbance at 620 nm. (Adapted from ref [25])

Table 1. Characteristics of the EPR effect of nanomedicine or macromolecular drugs

Biocompatibility	No interaction with blood components or blood vessels, no antigenicity, no clearance by the reticuloendothelial system, no cell lysis
Molecular size	Greater than 40 kDa (larger than the renal clearance threshold)
Surface charge	Weakly negative to near neutral
Time required to achieve	Longer than several hours in systemic circulation in mice
Drug retention time	Mostly days to weeks, in great contrast to passive targeting (in which low-MW molecules are rapidly cleared into the systemic circulation in a few min. cf. low molecular weight contrast agent (see text).

Table 2. Plasma clearance times of selected modified and native proteins in vivo

Protein	Species difference, original/test animal	Probe modification	pI[a]	MW (kDa)	$t_{1/2}$[b]	Note	Ref
• **Albumin**	Mouse/mouse	None	4.8	68	72–96 h	Native, syngeneic	[20,94]
Albumin	Mouse/mouse	DTPA (^{51}Cr)[d]	≦4.8	-	6 h	Slightly surface modified, loss of amino group, syngeneic	
Albumin	Cow/mouse	DTPA (^{51}Cr)[d]	≦4.8	-	1 h	Slightly surface modified, loss of amino group, xenogeneic	
Formaldehyde modified albumin	Human/rat	Formaldehyde ^{125}I	≦4.8	-	25 min	Denatured, loss of amino group, xenogeneic	
• **α_2-Macroglobulin**	Human/mouse	^{125}I	5.3	180×4	140 h	Native, xenogeneic	[20,94]
α_2-Macroglobulin-plasmin complex	Human/mouse	^{125}I	-	180×4	5 min	Inhibitor-protein complex, xenogeneic	
• **Immunoglobulin (IgG)**	Mouse/mouse	DTPA[d]	≦6.8	159	60 h	Slightly surface modified, loss of amino group, syngeneic	[20,94]
• **Interferon α**	Human/human	None		18	8 h (sc)[c]	$t_{1/2}$ 4 min	[20]
Pegylated interferon α2a	Human/human	PEG		52	80 h (sc)[c]		
• **Adenosine deaminase (ADA)**	Cow/mouse	None	4.9	38	<0.5 h	Native, xenogeneic	[95]
Pegylated ADA	Bovine/mouse	PEG[d]	-	>38	28 h, 3–6 days in humans	60% of primary amine conjugated with PEG (5000 Da), xenogeneic	
• **Arginine deiminase (ADI)**	*Mycoplasma hominis*/mouse	Native	5.5	46	<5 h	Native, xenogeneic	[96]
Pegylated ADI	*M. hominis*/mouse	PEG[d]	-	>46	~7 days	10–12 PEG (20,000 Da) attached to each ADI, xenogeneic	
• **Bilirubin oxidase, native**[d]	Microbial/mouse			52	0.25 h		[98,99]
Bilirubin oxidase PEG conjugate	Microbial/mouse			110	5 h		
• **D-amino acid oxidase native**	Pig/mouse			39	14 h		[41]
D-amino acid oxidase PEG conjugate	Pig/mouse			63	36 h		
• **Neocarzinostatin (NCS)**	*Streptomyces*/mouse	DTPA (^{51}Cr)[d]	3.4	12	1.8 min	Slightly surface modified, loss of amino group, xenogeneic	[20,94]
SMA-conjugated NCS (SMANCS)	*Streptomyces*/mouse	DTPA(^{51}Cr)[d], SMA	>3.0	17	19 min	Two chains of SMA (1200 Da) attached to each amino group of NCS; SMA is polyanionic, xenogeneic	

[a]Isoelectric point.
[b]Half-life in systemic circulation (minutes, hours, or days), given i.v. unless otherwise stated.
[c]From microbe, *Myrothecium verrucaria*
[d]DTPA or PEG was reacted with the primary amino group of a lysine residue or N-terminal residue, which made the group much less cationic.
[e]Subcutaneous.

Table 3. Selected parameters affecting plasma residence times of different nanoparticles

Type of nanoparticle	Test animal	ζ potential (mV)	Mean particle size (nm)	Plasma residence time		Remarks	Ref
				$T_{1/2}$	$T_{1/10}$		
• Liposome (nonpegylated)	Mouse	-7.31	124	9.08 h	>24 h	Doxorubicin loaded, DPPC:Chol = 1:1	[97]
Liposome, weakly cationic	Mouse	+5.58	131	4.51 h	15 h (mean)	Doxorubicin loaded, DPPC:Chol:DC-Chol = 5:4:1 slightly positive	
Liposome, strongly cationic	Mouse	+24.25	95	<30 min	<1 h	Doxorubicin loaded, DPPC:DC-Chol = 5:5 strongly positive	
• pLL-DNA complex	Mouse	Positive	-	<5 min	30 min	^{32}P-labeled 8-kbp DNA	[49]
• Chitosan nanoparticle weakly anionic	Mouse	-13.2	149.2	-	12 h (mean)	CMC/MMA = 1:2 slightly negative	[51]
Chitosan nanoparticle strongly anionic	Mouse	-38.4	156.0	-	3 h (mean)	CMC/MMA = 2:1 strongly negative	
Chitosan nanoparticle weakly cationic	Mouse	+14.8	150.1	-	<1 h	CH/MMA = 1:1 slightly positive	
Chitosan nanoparticle strongly cationic	Mouse	+34.6	152.7	-	<1 h	CH/MMA = 2:1 strongly positive	

Abbrebiations: DPPC: L-α-dipalmitoylphosphatidylcholine

Chol: cholesterol

DC-Chol: 3β-[*N*-(*N'*,*N'*-dimethylaminoethyl)carbamoyl]cholesterol

pLL: poly(L-lysine)

CMC: carboxymethyl chitosan

MMA: methyl methacrylate

CH: chitosan hydrochloride

Journal of Controlled Release 165 (2013) 191–198

Contents lists available at SciVerse ScienceDirect

Journal of Controlled Release

journal homepage: www.elsevier.com/locate/jconrel

Micelles of zinc protoporphyrin conjugated to *N*-(2-hydroxypropyl)methacrylamide (HPMA) copolymer for imaging and light-induced antitumor effects in vivo

Hideaki Nakamura [a,b], Long Liao [a], Yuki Hitaka [a], Kenji Tsukigawa [a], Vladimir Subr [c], Jun Fang [a,b], Karel Ulbrich [c], Hiroshi Maeda [a,*]

[a] Research Institute for Drug Delivery System, Faculty of Pharmaceutical Science, Sojo University, Kumamoto, Japan
[b] Laboratory of Microbiology and Oncology, Faculty of Pharmaceutical Science, Sojo University, Kumamoto, Japan
[c] Institute of Macromolecular Chemistry, Academy of Sciences of the Czech Republic, Prague, Czech Republic

ARTICLE INFO

Article history:
Received 19 September 2012
Accepted 25 November 2012
Available online 3 December 2012

Keywords:
Fluorescence imaging
Fluorescent nanoprobe
Singlet oxygen
Tumor targeting
HPMA-ZnPP conjugate
EPR effect

ABSTRACT

We synthesized *N*-(2-hydroxypropyl)methacrylamide polymer conjugated with zinc protoporphyrin (HPMA-ZnPP) and evaluated its application for tumor detection by imaging and treatment by light exposure using in mouse sarcoma model. To characterize HPMA-ZnPP micelle, we measured its micellar size, surface charge, stability, photochemical, biochemical properties and tissue distribution. In vivo anti-tumor effect and fluorescence imaging were carried out to validate the tumor selective accumulation and therapeutic effect by inducing singlet oxygen by light exposure. HPMA-ZnPP was highly water soluble and formed micelles spontaneously having hydrophobic clustered head group of ZnPP, in aqueous solution, with a hydrodynamic diameter of 82.8 ± 41.8 nm and zeta-potential of + 1.12 mV. HPMA-ZnPP had a long plasma half-life and effectively and selectively accumulated in tumors. Although HPMA-ZnPP alone had no toxicity in S-180 tumor-bearing mice, light-irradiation significantly suppressed tumor growth in vivo, similar to the cytotoxicity to HeLa cells in vitro upon endoscopic light-irradiation. HPMA-ZnPP can visualize tumors by fluorescence after i.v. injection, which suggests that this micelle may be useful for both tumor imaging and therapy. Here we describe preparation of a new fluorescence nanoprobe that is useful for simultaneous tumor imaging and treatment, and application to fluorescence endoscopy is now at visible distance.

1. Introduction

Photodynamic therapy (PDT) employs a photosensitizer and cytotoxic light-induced singlet oxygen ($^1O_2$) generation. $^1O_2$ generation damages DNA, RNA, proteins and lipids, which leads to cell death. Porphyrin derivatives usually generate cytotoxic $^1O_2$ after light irradiation that corresponds to the absorption wavelength of porphyrin derivatives [1–3]. Laserphyrin® and Photofrin® and others are well known porphyrin derivatives that are approved for limited use in conventional clinical PDT for early-stage lung (bronchogenic) or superficial cancer accessible to exciting light (laser irradiation at 630 nm) [4,5]. However, small molecular photosensitizers are expected to be distributed throughout the body including skin and other organs, and most have limited tumor selectivity or tumor-imaging capacity. Thus, they would cause cutaneous hyper-photosensitivity as the major adverse effect, which limits therapeutic success.

To solve this problem, one can utilize macromolecular photosensitizers, which have much longer half-lives in circulation and gradually and selectively accumulate in tumor tissues because of the EPR (enhanced permeability and retention) effect, accompanying much less accumulation in normal tissue [6–11]. Our group previously reported that biocompatible macromolecules (MW >40 kDa) showed the EPR effect and accumulated selectively in tumors [6,12,13]. For the EPR effect to operate, the macromolecular surface charge is as important a determinant as is molecular size; a neutral to slightly negative charge and MW of >40 kDa are preferable for tumor targeting [6,12,14]. In this study, we utilized a conjugate of zinc protoporphyrin (ZnPP) and 12-kDa *N*-(2-hydroxypropyl)methacrylamide (HPMA) copolymer, which has a neutral charge and is highly biocompatible. The conjugate behaved as a large macromolecule (apparent MW is 198-kDa), as do many polymer conjugates of low-molecular-weight micellar drugs that show preferential tumor accumulation [15–18].

Light-irradiated (at 420 nm, absorption max of ZnPP) ZnPP effectively generates $^1O_2$ and thereby exhibits potent cytotoxicity [18,19]. ZnPP is also a potent inhibitor of heme oxygenase-1 (HO-1), or HSP-32, which is a survival factor. HO-1 is highly upregulated in many cancer tissues in vivo and confers an antioxidative function to cells. Therefore, inhibition of HO-1 by ZnPP makes tumor cells more vulnerable to oxystress, the result being selective tumor regression. Most of normal cells are not affected because HO-1 in normal cells is expressed only at low level and insignificant. However, ZnPP is highly hydrophobic and soluble only in alkaline solutions or organic solvents. This

* Corresponding author at: Institute for DDS, Sojo University, Ikeda 4-22-1, Kumamoto, 860-0082, Japan. Tel.: +81 96 326 4114; fax: +81 96 326 3185.
E-mail address: hirmaeda@ph.sojo-u.ac.jp (H. Maeda).

0168-3659/$ – see front matter © 2012 Elsevier B.V. All rights reserved.
http://dx.doi.org/10.1016/j.jconrel.2012.11.017

insolubility of ZnPP in physiological aqueous solution hampers its therapeutic application. To overcome this obstacle, we developed water-soluble ZnPP micelles: one is styrene maleic acid copolymer (SMA) micelles that encapsulate ZnPP and forms nanomicelles (SMA-ZnPP), the other is pegylated ZnPP (PEG-ZnPP) [18–22]. Both ZnPP micelles alone exhibited antitumor activity, and light irradiation greatly enhanced this activity [18]. Despite high tumor accumulation of PEG-ZnPP and significant antitumor activity, the maximum ZnPP loading in PEG-ZnPP is theoretically about 6% (wt/wt), so the intravenous (i.v.) dose of PEG-ZnPP may become several grams to achieve therapeutic concentrations. Although ZnPP loading of SMA-ZnPP can be increased to about 50%, SMA-ZnPP micelles tended to accumulate predominantly in the liver and spleen [23]. Therefore, we aimed to develop another type of ZnPP micelles with greater tumor targeting and adequate loading of ZnPP.

Here, we describe the synthesis of HPMA-ZnPP, which spontaneously formed micelles in aqueous solution. We examined its size distribution, spectroscopic property, micelle stability, generation of $^1O_2$, cellular uptake, tumor and tissue distribution and antitumor activity in vivo when used with xenon light-irradiation. Other important results concern simultaneous in vivo fluorescence imaging of the whole animal from outside, and the therapeutic effect of the polymer-photosensitizer conjugate.

2. Materials and methods

2.1. Materials

Male ddY mice were purchased from Kyudo Co., Ltd, Saga, Japan. Protoporphyrin IX, zinc acetate, triethylamine, dimethylaminopyridine, diethylether, Tween 20 and egg lecithin of reagent grade were purchased from Wako Pure Chemical, Osaka, Japan. 1-Ethyl-3-(3-dimethylaminopropyl)carbodiimide and 3-(4,5-dimethyl-2-thiazolyl)-2,5-diphenyl-2H-tetrazolium bromide (MTT) were purchased from Dojindo Chemical Laboratory, Kumamoto, Japan. 2,2,6,6-Tetramethyl-4-piperidone (4-oxo-TEMP) was purchased from Tokyo Chemical Industry, Tokyo, Japan. The HPMA polymer (mean MW ~12 kDa) we used contains one free amino group at the end, and was prepared at the Institute of Macromolecular Chemistry, Prague, Czech Republic.

2.2. Synthesis of HPMA-ZnPP

Scheme 1 shows the synthesis of HPMA-ZnPP conjugate, in which conjugation of carboxyl group of free ZnPP with either hydroxyl group or amino group of HPMA (mean MW 12 kDa) was carried out to form ester and amide bonds, respectively. In brief, 570 mg of HPMA as Scheme 1 and 281 mg of ZnPP were mixed in 50 ml of DMSO at 50 °C and reacted by addition of 1.0 g of triethylamine, 1.2 g of dimethylaminopyridine and 1.9 g of 1-ethyl-3-(3-dimethylaminopropyl)carbodiimide hydrochloride as a catalyst for 12 h at 50 °C in the dark. After the reaction, HPMA-ZnPP conjugates were precipitated by addition of diethylether (200 ml), and reaction catalyst in the supernatant was removed by centrifugation. The conjugates were washed three times with diethylether to remove the reaction catalyst and DMSO. HPMA-ZnPP was purified via gel permeation chromatography (Bio-Beads SX-1, BioRad, Hercules, CA) using dimethylformamide (DMF) as elute. Peak fraction of elutes was ultrafiltrated with membrane filter with a cutoff molecular size of 100 kDa, to remove decomposed or unreacted small molecules and to replace the DMF to distilled water. Fluffy powder (635 mg) was obtained by lyophilization.

2.3. Gel permeation column chromatography

Analytical gel permeation column chromatography of HPMA-ZnPP was performed with Bio-Beads SX-1 using a column ($\varphi = 2.5$ cm, L = 60 cm) and eluted with DMF at a flow rate of 0.1 ml/min. 1.5 ml fractions of elutes were measured at absorbance at 422 nm, which corresponded to ZnPP absorbance.

2.4. Fluorescence spectroscopy and fluorescence polarization

HPMA-ZnPP at 10 μg/ml was dissolved in PBS containing Tween 20 (0.0005–0.5%) or urea (1–9 M), and fluorescence spectra were measured with a fluorescence spectrophotometer (FP-6600; JASCO, Tokyo). HPMA-ZnPP (2.5 μg/ml) or free ZnPP (0.5 μg/ml) was dissolved in DMF, and sample solutions were then excited at 420 nm by a fixed polarized light; fluorescence emission at 590 nm was recorded at parallel (0°) and perpendicular (90°) angles of the secondary polarizer, which was equipped in a Model FP-6600 fluorescence spectrophotometer. The fluorescence polarization value (P value) was calculated by using the equation $P = (I_{//} - I_{\perp})/(I_{//} + I_{\perp})$, where $I_{//}$ = fluorescence intensity of the parallel component and $I_{\perp}$ = fluorescence intensity of the perpendicular component. The fluorescent polarization value is proportional to the molecular size of the fluorescent probe [24].

2.5. High performance liquid chromatography (HPLC)

Cleavage of ester bond of this conjugate HPMA-ZnPP was analyzed by using HPLC (Prominence, Shimadzu, Kyoto, Japan) with the multimode size exclusion column GF-310 HQ (300×7.5 mm) with photodiode array detection at 422 nm, which was eluted with a mixture of 30% DMSO and 70% methanol containing 10 ppm trifluoroacetic acid at 1.0 ml/min.

2.6. Dynamic light scattering and zeta potential

HPMA-ZnPP or HPMA was dissolved in 0.01 M phosphate-buffered 0.15 M saline (PBS, pH 7.4) at 1 mg/ml and was filtered through a 0.2 μm filter attached to a syringe. The particle size and surface charge (zeta potential) were measured by light scattering (ELS-Z2; Otsuka Photal Electronics Co. Ltd., Osaka).

2.7. Transmission electron microscopy (TEM)

A drop of HPMA-ZnPP (0.1 mg/ml) was applied to a copper grid coated with carbon film and air-dried. The micelle image and size of

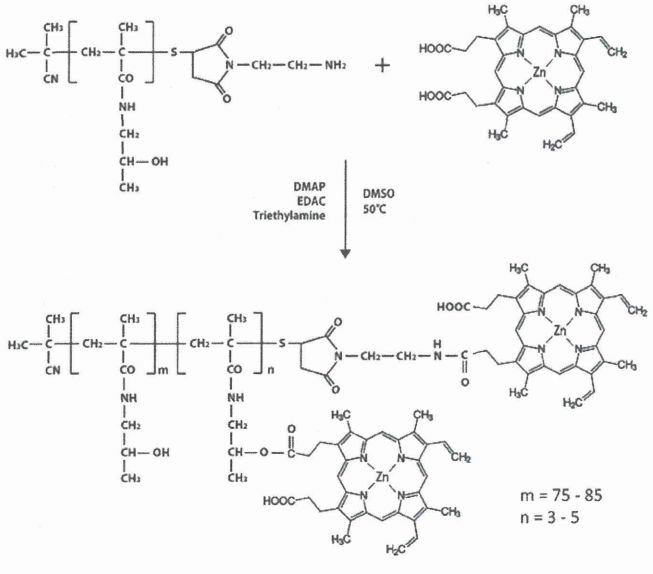

Scheme 1. HPMA-ZnPP synthesis. Chemical structures and conjugation pathway. ZnPP was conjugated to the secondary hydroxyl group and the terminal amino group of HPMA.

HPMA-ZnPP were analyzed by using a transmission electron microscope (Tecnai F20; FEI, Hillsboro, OR).

2.8. Electron spin resonance (ESR) spectroscopy

ESR spectra were measured by using an ESR spectrometer at 25 °C (JES FA-100; JEOL, Tokyo). Sample solutions containing 200 μg/ml HPMA-ZnPP (or 40 μg/ml ZnPP) and 20 mM 4-oxo-TEMP with or without light irradiation were evaluated. Samples in a flat quartz cell (Labotec, Tokyo) were irradiated (28 mW/cm^2) by using xenon light at 400–800 nm (MAX-303; Asahi Spectra, Tokyo) for indicated times. The ESR spectrometer was usually set at a microwave power of 1.0 mW, amplitude of 100-kHz and field modulation width of 0.1 mT.

2.9. Cytotoxicity assay

HeLa cells were maintained in DMEM supplemented with 10% fetal calf serum under 5% CO_2/air at 37 °C. HPMA-ZnPP or ZnPP was added 24 h after plating HeLa cells at 3000 per well in 96-well plates. Irradiation with fluorescent blue light having peak emission at 420 nm (TL-D; Philips, Eindhoven, Netherland) with 1.0 J/cm^2 per 15 min was then performed. After 48 h of culture, the MTT assay was carried out to quantify viable cells, with absorbance at 570 nm as described by instruction of the manufacture.

2.10. Intracellular uptake

HPMA-ZnPP or free ZnPP was added at a concentration of 20 μg ZnPP equivalent/ml 48 h after plating HeLa cells at 25,000 cells per well in 24-well plates (1.9 cm^2/well). At indicated time periods, cells were washed with PBS and added with 2 ml ethanol followed by sonication (20 W, 30 s) to extract the HPMA-ZnPP or free ZnPP. Concentration of ZnPP was measured by fluorescence intensity (Ex. 422 nm, Em. 590 nm).

2.11. In vivo antitumor activity

The care and maintenance of animals were undertaken in accordance with the institutional guidelines of the Institutional Animal Care and Use Committee of Sojo University. Mouse sarcoma S-180 cells (2×10^6 cells) were implanted s.c. in the dorsal skin of ddY mice. When tumor reached to diameter of about 5 mm, 15 mg/kg of ZnPP equivalent drugs in saline was injected i.v. Then after 24, 48 and 72 h, tumor was irradiated by xenon light (MAX-303; Asahi Spectra) at 400–800 nm (20 mW/cm^2) for 5 min as described. Tumor volume (mm^3) was calculated as $(W^2\times L)/2$ by measuring the length (L) and width (W) of the tumor on the dorsal skin.

2.12. Pharmacokinetics and tissue distribution of HPMA-ZnPP

When S-180 tumor in mice with tumor diameter of approximately 10 mm, injected i.v. was 15 mg of ZnPP equivalent per kg of free ZnPP or HPMA-ZnPP. At the indicated times, mice were killed, perfused with physiological saline and dissected, and then tissues were weighed, DMSO (1 ml per 100 mg of tissue) was added, and samples were homogenized and centrifuged (12,000 g, 25 °C, 10 min) to precipitate insoluble tissue debris, and ZnPP and HPMA-ZnPP in the supernatant were quantified by fluorescence intensity (excitation at 422 nm, emission at 590 nm).

2.13. In vivo fluorescence imaging

Tumor-bearing mice as described above were injected with 15 mg of ZnPP (equivalent) per kg i.v. At 24 h after injection, mice were shaved and, under isoflurane gas anesthesia, were subjected to in vivo fluorescence imaging using IVIS XR (Caliper Life Science, Hopkinton, MA) (excitation at 430 ± 15 nm and emission at 695–770 nm). Fluorescent images of each tissue were also observed after dissection.

3. Results

3.1. Synthesis of HPMA-ZnPP

The carboxyl group of ZnPP was conjugated to HPMA at the secondary hydroxyl group and the terminal amino group (Scheme 1). Gel permeation chromatography of the reaction product on Bio-beads column showed that HPMA-ZnPP had a higher molecular weight than free ZnPP, and neither free ZnPP nor decomposition product was detected (Fig. 1A). The total yield was 47% (wt/wt) based on ZnPP. The macromolecular characteristics of HPMA-ZnPP were also examined by fluorescence polarization. The polarization value (P value) of free ZnPP in dimethylformamide (DMF) was 0.0064, whereas that of HPMA-ZnPP was 0.0378, which suggests that HPMA-ZnPP had a higher molecular weight than ZnPP (Fig. 1B). Also HPMA-ZnPP was shown to have good water solubility of more than 30 mg/ml in water. The ZnPP content in HPMA-ZnPP was estimated as 20% (wt/wt) on the basis of absorbance of ZnPP.

3.2. Micellar structure of HPMA-ZnPP

ZnPP is highly hydrophobic and is believed to form aggregates in water by π–π stacking interactions between tetrapyrrole planes. Thus, we anticipated that HPMA-ZnPP would form micellar structures in aqueous solution; namely ZnPP containing head group can form a hydrophobic inner core as clustered head group, and a hydrophilic HPMA chain as tail would form an outer surface layer facing toward water. Fig. 1C shows that either amide or ester bonds between HPMA and ZnPP are stable in DMSO and in alkaline pH (10 mM NaOH) without DMSO, separately. However, alkaline treatment in DMSO efficiently cleaved HPMA-ZnPP since the micellar structure is disintegrated in organic solvent (DMSO), and OH− becomes accessible to ester bond and resulted in hydrolyzes of ester bond and release of free ZnPP. Dynamic light scattering analyses showed that in aqueous solution of HPMA-ZnPP it formed large micelles particles (hydrodynamic diameter: 82.8 ± 41.8 nm), which suggests that HPMA-ZnPP was associated into micelles in aqueous solution, whereas HPMA alone had a hydrodynamic diameter of 5.6 ± 1.9 nm (Fig. 1D). Transmission electron microscopy also showed the micelle size of HPMA-ZnPP as 30–80 nm (Fig. 1E). HPMA-ZnPP micelles in phosphate-buffered saline (PBS) showed almost neutral zeta potential (+1.12 mV).

3.3. HPMA-ZnPP formed micelles via hydrophobic interaction

ZnPP has a λ_{max} at 422 nm in organic solvents such as DMSO and ethanol, and it exists as monodispersed free molecules. However, when free ZnPP molecules aggregate with each other in soluble form in aqueous solution, the λ_{max} shifts towards a shorter wavelength (390 nm). This blue shift was also observed when HPMA-ZnPP was dissolved in aqueous solution (Fig. 1F). Furthermore, the blue shift decreased after adding detergent or Tween 20, or when dissolved in DMSO, but not in the presence of 9 M urea (Fig. 1F). Measurement of fluorescence intensity of HPMA-ZnPP revealed the same phenomenon; HPMA-ZnPP fluorescence was quenched in aqueous solution, which indicates a hydrophobic interaction among aromatic rings or π–π stacking of ZnPP, whereas HPMA-ZnPP fluorescence intensity was restored by adding detergent but not 9 M urea (Fig. 1G, H).

3.4. Demonstration of $^1O_2$ generation from HPMA-ZnPP

The $^1O_2$-generating capacity of HPMA-ZnPP was examined by means of ESR spectroscopy with the use of spin-trapping agent